ORIGINAL RESEARCH

CNS Embryonal Tumor with PLAGL Amplification, a New Tumor Type in Children and Adolescents: Insights from a Comprehensive MRI Analysis

Tietze A[1], Bison B[2,3], European Society for Paediatric Oncology (SIOPE)-Brain Tumour Group[4], Engelhardt J[5,6], Fenouil T[7], Figarella-Branger D[8], Goebell E[9], Hakumäki J[10,11], Koscielniak E[12], Ludlow LE[13,14,15], Meyronet D[7], Nyman P[16, 17], Øra I[18], Pesola J[19], Rauramaa T[20], Reddingius RE[21], Samuel D[22], Sexton-Oates A[23], Vasiljevic A[7], Wefers AK[24,25], Zamecnik J[26], Jones DTW[27,28,29], Keck MK[27,28,29#], von Hoff K[30,31#]

ABSTRACT

BACKGROUND AND PURPOSE: CNS embryonal tumor with *PLAGL1*/*PLAGL2* amplification (ET, PLAGL) is a newly identified, highly malignant pediatric tumor. Systematic MRI descriptions of ET, PLAGL are currently lacking.

MATERIALS AND METHODS: MRI data from 19 treatment-naïve patients with confirmed ET, PLAGL were analyzed. Evaluation focused on anatomical involvement, tumor localization, MRI signal characteristics, DWI behavior, and the presence of necrosis and hemorrhage. Descriptive statistics (median, interquartile range, percentage) were assessed.

RESULTS: Ten patients had *PLAGL1* and nine *PLAGL2* amplifications. The solid components of the tumors were often multinodular with heterogeneous enhancement (mild to intermediate in 47% and intermediate to strong in 47% of cases). Non-solid components included cysts in 47% and necrosis in 84% of the cases. The tumors showed heterogeneous T2WI hyper- and isointensity (74%), relatively little diffusion restriction (ADC values < contralateral normal-appearing WM in 36% of cases with available DWI), and tendencies towards hemorrhage/calcification (42%). No reliable distinction was found between *PLAGL1*- and *PLAGL2*- amplified tumors or compared to other embryonal CNS tumors.

CONCLUSIONS: The study contributes to understanding the imaging characteristics of ET, PLAGL. It underscores the need for collaboration in studying rare pediatric tumors and advocates for the use of harmonized imaging protocols for better characterization.

ABBREVIATIONS: ATRT= atypical teratoid/rhabdoid tumor; ETMR= embryonal tumor with multilayered rosettes; ET, PLAGL= CNS embryonal tumor with PLAGL amplification; EVD= external ventricular drain; IQR: interquartile range; *PLAGL1*= pleomorphic adenoma gene-like 1; *PLAGL2*= pleomorphic adenoma gene-like 2; WHO= World Health Organization

Received month day, year; accepted after revision month day, year.
From the Inst. of Neuroradiology, Charité - Universitätsmedizin Berlin, corporate member of Freie Universität Berlin and Humboldt-Universität zu Berlin, Germany (T.A.); Dept. of Neuroradiology, University Hospital Augsburg, Germany (B.B.); Neuroradiological Reference Center for the pediatric brain tumor (HIT) studies of the German Society of Pediatric Oncology and Hematology, Faculty of Medicine, University Augsburg, Augsburg, Germany (B.B.); Service de Neurochirurgie B, CHU de Bordeaux, University of Bourdeaux, France (E.J.); Univ. Bordeaux, Bordeaux INP, CNRS, IMB, UMR 5251, Talence, France (E.J.); Institut de Pathologie Multisite-Site Est, Groupement Hospitalier Est, Hospices Civils de Lyon, Lyon, France (F.T., M.D., V.A.); Aix-Marseille Univ, APHM, CNRS, INP, Inst Neurophysiopathol, CHU Timone, Service d'Anatomie Pathologique et de Neuropathologie, Marseille, France (F-B.D.); Dept. of Diagnostic and Interventional Neuroradiology, University Medical Center Hamburg-Eppendorf, Hamburg, Germany (G.E.); Dept. of Clinical Radiology, Kuopio University Hospital, Kuopio, Finland (H.J.); Inst. of Clinical Medicine, University of Eastern Finland, Kuopio, Finland (H.J.); Dept. of Pediatric Oncology/Hematology/Immunology, Olgahospital, Klinikum Stuttgart, Stuttgart, Germany (K.E.); Murdoch Children's Research Inst., The Royal Children's Hospital, Flemington Road, Parkville, Victoria, Australia (L.LE); Children's Cancer Centre, The Royal Children's Hospital, Flemington Road, Parkville, Victoria, 3052, Australia (L.LE); Dept. of Paediatrics, The University of Melbourne, Parkville, Victoria, Australia (L.LE); Crown Princess Victoria Children´s Hospital, Linköping University Hospital, Linköping, Sweden (N.P.); Dept. of Biomedical and Clinical Sciences, Linköping University, Linköping, Sweden (N.P.); Dept. of Pediatric Oncology and Hematology, Skåne University Hospital, Lund University, Lund, Sweden (Ø.I); Dept. of Pediatrics, Pediatric Hematology and Oncology Ward, Kuopio University Hospital and Inst. of Clinical Medicine, University of Eastern Finland, Kuopio, Finland (P.J.); Dept. of Clinical Pathology, Kuopio University Hospital and Unit of Pathology, Inst. of Clinical Medicine, University of Eastern Finland, Kuopio, Finland (R.T.); Dept. of Neuro-Oncology, Princess Máxima Center for Pediatric Oncology, Utrecht, The Netherlands (R.RE.); Dept. of Hematology-Oncology, Valley Children's Hospital, Madera, CA, USA (S.D.); Rare Cancers Genomics Team, Genomic Epidemiology Branch, International Agency for Research on Cancer/World Health Organization, Lyon, France (S-O.A.); Inst. of Neuropathology, University Medical Center Hamburg-Eppendorf, Hamburg, Germany (W.A.K.); Mildred Scheel Cancer Career Center HaTriCS4, University Medical Center Hamburg-Eppendorf, Hamburg, Germany (W.A.K.); Dept. of Pathology and Molecular Medicine, Second Faculty of Medicine, Charles University and University Hospital Motol, Prague, Czech Republic (Z.J.); Division of Pediatric Glioma Research, Hopp Children's Cancer Center Heidelberg (KiTZ), Heidelberg, Germany (J.D.T.W., K.M.K.); Division of Pediatric Glioma Research (B360), German Cancer Research Center (DKFZ), Heidelberg, Germany (J.D.T.W., K.M.K.); National Center for Tumor Diseases (NCT), NCT Heidelberg, a partnership between DKFZ and Heidelberg University Hospital, Germany (J.D.T.W., K.M.K.); Dept. of Pediatric Oncology and Hematology, Charité-Universitätsmedizin Berlin, Corporate Member of Freie Universität Berlin, Humboldt-Universität zu Berlin, and Berlin Inst. of Health, Berlin, Germany (V.H.K.); Dept. of Paediatric and Adolescent Medicine, Aarhus University Hospital, Aarhus, Denmark (V.H.K.); (European Society for Paediatric Oncology (SIOPE)-Brain Tumour Group.
# These authors contributed equally

Disclosure of potential conflicts of interest: Where authors are identified as personnel of the IARC/WHO, the authors alone are responsible for the views expressed in this article and they do not necessarily represent the decisions, policy, or views of the IARC/WHO.
Zapotocky M: travel grant and advisory board AstraZeneca

Corresponding author:
Anna Tietze (ORCID 0000-0002-2601-9055)
Institute of Neuroradiology
Tel.: +49 30 450657253
e-mail: anna.tietze@charite.de
Charité - Universitätsmedizin Berlin, corporate member of Freie Universität Berlin and Humboldt-Universität zu Berlin
Augustenburger Platz 1
D - 13353 Berlin, Germany

SUMMARY SECTION

PREVIOUS LITERATURE: CNS embryonal tumor with PLAGL1/PLAGL2 amplification (ET, PLAGL) is a recently defined pediatric tumor characterized by a specific methylation profile and molecular features. A comprehensive re-analysis of tumor tissue of 32 patients, initially diagnosed with medulloblastomas, other embryonal tumors, or high-grade gliomas, led to the characterization of this distinct tumor type, which is not yet included in the 2021 edition of the WHO Classification of CNS Tumors. So far, a radiological description in a larger cohort has been lacking. MRI data from 19 patients were collected from 16 international centers, providing imaging findings of this new tumor.

KEY FINDINGS: MRI revealed heterogeneous T2WI hyper-/isointensity, similar to other rare embryonal tumors. However, diffusion restriction was less pronounced. The tumors often contained cystic and/or necrotic areas, showed heterogeneous enhancement, and occasionally presented with hemorrhage and/or calcifications. Only one tumor showed a metastasis at diagnosis.

KNOWLEDGE ADVANCEMENT: In our cohort, ET, PLAGL could not be clearly distinguished from other embryonal tumors, and no differences were observed between PLAGL1- and PLAGL2-amplified tumors. This study contributes to the imaging characterization of emerging tumor entities within the increasingly detailed tumor classification. It underscores the need for collaboration between centers to enhance our understanding of new, rare tumors.

INTRODUCTION

The molecular and histological diversity of CNS tumors is increasingly recognized as reflected in the recent 2021 WHO Classification of CNS Tumors that integrates histology, immunohistochemistry, and molecular features to arrive at a final integrated diagnosis (1). The primary aim of this refined tumor classification is to improve diagnostic and prognostic accuracy, tailor treatment strategies more effectively, and ultimately pave the way for the development of targeted therapies.

Recent advances in DNA methylation profiling, copy number analysis, and DNA/RNA sequencing have led to significant refinement in the classification of CNS tumors, including the identification of new tumor types and subtypes (2-4). An example of a new type is the CNS embryonal tumor with PLAGL amplification (ET, PLAGL), a rare type of embryonal tumor mainly seen in children and adolescents, which was first described in 2023 and is not yet included in the WHO classification of CNS tumors (4). Within the category of embryonal tumors, the 2021 WHO Classification of CNS Tumors distinguishes the more common medulloblastoma subgroups from other, rare embryonal tumors such as the atypical teratoid/rhabdoid tumors (ATRT), embryonal tumors with multilayered rosettes (ETMR), and embryonal tumor NOS, among which ET, PLAGL has recently been reported as a distinct tumor type. Alterations in the pleomorphic adenoma gene 1 (PLAG1) are linked to the overexpression of transcriptional factors, playing a crucial role in the development of various tumors including pleomorphic adenomas of the salivary gland, lipoblastomas, hepatoblastomas, and some leukemias (5). Of the three PLAG family genes (PLAG1, PLAGL1, and PLAGL2), PLAGL1 and PLAGL2 are specifically linked to CNS embryonal tumors through gene amplification and resultant overexpression of PLAGL1 or PLAGL2. This amplification leads to alterations in associated downstream genes such as imprinted genes and/or potential drug targets (4). We recently reanalyzed tumor samples from 31 patients, whose tumors were initially either not classifiable or diagnosed as medulloblastoma, other embryonal tumors, sarcoma, or high-grade glioma, and identified ET, PLAGL as a distinct pediatric tumor category. Amplifications of PLAGL1 were primarily found in school-aged children and adolescents (median age 10.5 years), while PLAGL2 amplifications were more common in younger children (median age 2 years) (4).

Currently, there is limited knowledge regarding the outcomes of patients with ET, PLAGL. This uncertainty is compounded by the different treatment strategies given across patients so far (4). Some received radiation therapy (local or as a craniospinal irradiation), others were treated with high-dose chemotherapy, and some underwent both. In the study by Keck et al., a significant difference in overall survival rates was observed between patients with PLAGL1-amplified tumors and those with PLAGL2-amplified tumors (with 5-year overall survival rates of 66% and 25%, respectively) with female patients demonstrating a marginally better outcome, though these results were not statistically significant. Additionally, PLAGL1 amplifications were more commonly found in female patients compared to PLAGL2 amplifications (4).

The updated CNS tumor classification necessitates a revised radiological characterization of both reclassified and newly identified tumor entities to facilitate accurate presurgical diagnoses, growth patterns, and clinical characteristics. The objective of our study was therefore to characterize ET, PLAGL radiologically using conventional MRI data of 19 patients. The hypothesis was that the imaging characteristics of ET, PLAGL would resemble those of other embryonal tumors and that differences between PLAGL1- and PLAGL2-amplified tumors would be observable. The MRI data for this rare tumor were collected from multiple international centers and analyzed by two experienced pediatric neuroradiologists through consensus, applying established conventional imaging criteria (6). Results are presented as descriptive summaries along with illustrations of typical imaging findings.

MATERIALS AND METHODS

Patients

Pseudonymized, pretreatment imaging data of 19 patients with proven ET, PLAGL were provided for central review either by the respective local center or by the national radiology reference center according to the available consent and local ethics vote. The majority (n=15) of these patients were part of the initial study on these tumors conducted by Keck et al. (4). Additionally, four patients diagnosed or re-classified as ET, PLAGL subsequently were included in the present cohort.

MRI Analysis

The MRI data were jointly evaluated in online meetings by two pediatric neuroradiologists (BB with 19 years, AT with 14 years of experience). They reached consensus decisions on pseudonymized images regarding the following imaging characteristics: 1. anatomic structures involved; 2. cortical, supratentorial WM, and deep GM involvement; 3. degree of perifocal edema, categorized as none, maximum 3 mm, less than 2 cm, or more than 2 cm; 4. degree of hydrocephalus, categorized as none, mild with ventricular dilation, moderate with ventricular dilation and periventricular edema, or severe with additional sulcal effacement, 5. infiltration of or proximity to the ventricular system (without normal tissue between tumor and ventricular wall), 6. volume calculated as (craniocaudal x transverse x anterior-posterior diameter)/2 (an approximation of the spherical model: (4/3) x π x (craniocaudal/2 x transverse/2 x anterior-posterior/2)); 7. T2WI intensity compared to unaffected cortex; 8. T1WI intensity compared to unaffected cortex; 9. FLAIR intensity compared to unaffected cortex; 10. ADC ratios (ROI with lowest intralesional ADC_{mean}/ROI with ADC_{mean} in contralateral normal-appearing WM; the same applies to ADC_{min} and ADC_{max} values); 11. presence of susceptibility indicating calcification and/or hemorrhage on gradient-echo imaging (T2* or SWI), potentially further specified by T1WI and T2WI; 12. extent of enhancement, categorized in 6 ranges (0%, 0%–25%, 25%–50%, 50%–75%, 75%–100%, or 100% of the solid tumor component); 13. strength of enhancement compared to the venous sinus (none, predominantly mild to intermediate, predominantly intermediate to strong); 14. skull involvement and/or scalloping; 15. presence of nonsolid components, such as thin-walled cysts and/or necrotic regions, the latter showing irregular, thick walls; 16. dissemination of tumor.

Descriptive statistics were used including median/interquartile range (IQR). All other variables were reported as percentages.

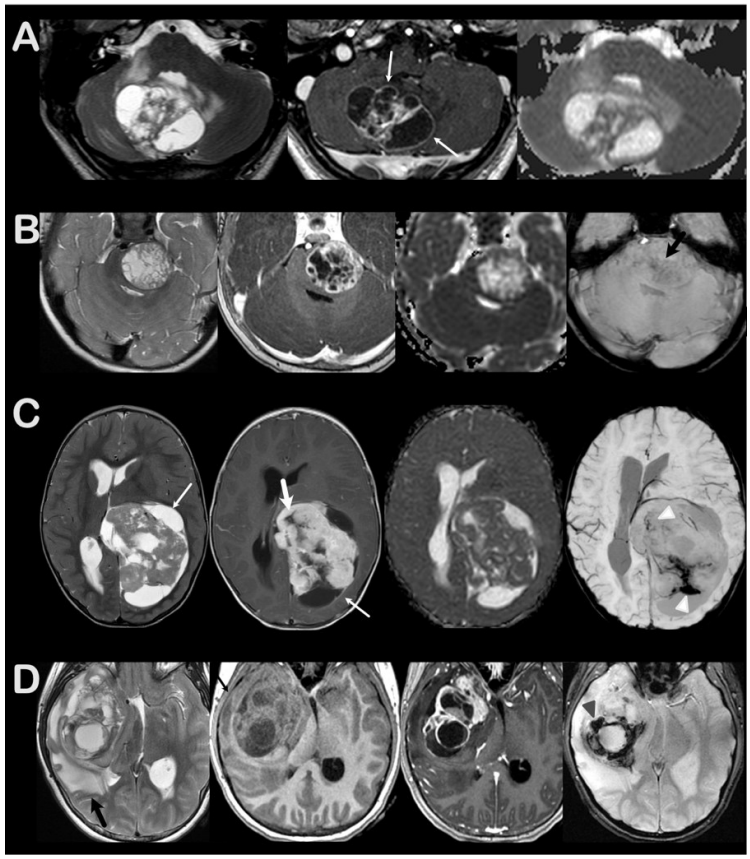

FIG 1. A: 18-year-old boy with a PLAGL1-amplified tumor in the right cerebellar hemisphere and the vermis with thin-walled cysts of different sizes (white arrows, second image). The solid parts are sparse, predominantly T2WI isointense and show heterogeneous, intermediate enhancement. There is no convincing diffusion restriction in the few, solid components (ADC_{mean} ratio 1.51). (From left to right: T2WI, contrast enhanced T1WI, ADC).

B: 17-month-old boy with a well-demarcated, PLAGL1-amplified tumor in the left side of the pons, extending into the cerebello-pontine angle and the prepontine cistern. The tumor contains numerous small, thick-walled, non-solid parts that mainly represent necroses, has no perifocal edema, and no clear diffusion restriction(ADC_{mean} ratio 1.07). The solid components are T2WI iso- to hyperintense and show intermediate to strong enhancement. There are very subtle susceptibilities (black arrow on last image) that may arise from hemorrhage or calcification. (From left to right: T2WI, contrast enhanced T1WI, ADC, T2*).

C: 16-month-old girl with a large, multi-lobulated, PLAGL2-amplified tumor in the left parietal lobe infiltrating the left lateral

ventricle. The non-solid parts are both thin- and thick-walled (thin and thick, white arrows, first and second image) and represent both tumor cysts and necroses. The solid parts are T2WI iso- to hypointense and show intermediate to strong enhancement. ADC values are comparable to those in normal tissue (third image; ADC_{mean} ratio 1.14), and there are susceptibilities in parts of the tumor (arrowheads, fourth image). (From left to right: T2WI, contrast enhanced T1WI, ADC, SWI).

D: 14-year-old girl with a right temporal, PLAGL1-amplified tumor with strong perifocal edema (black arrow, first image), thinning of the temporal bone (thin black arrow, second image), intermediate to strong enhancement, and extensive susceptibilities (grey arrowhead, last image). (From left to right: T2WI, T1WI without and with contrast, SWI).

RESULTS

Patients

Ten (53%) patients had PLAGL1 and 9 (47%) PLAGL2 amplifications. As previously known, a higher proportion of girls was observed in the PLAGL1 group, constituting 70% of the patients, compared to 33% in the PLAGL2 group. Detailed information regarding the patients' sex, age, and PLAGL status is provided in Tab. 1.

Imaging

Brain MRI data were available for all patients. Additionally, 12 patients had spinal MRI scans, and one patient also underwent a brain CT. The MRI datasets predominantly consisted of T2WI, T1WI with and without gadolinium contrast, and FLAIR sequences. DWI was available for 16 patients, T2* for 7, and SWI for 2 patients. Pseudo-continuous Arterial Spin Labeling (pCASL) was conducted for one patient, and MRS was performed on three patients (single-voxel, with echo times of 35ms, 135ms, and 144ms).

One patient, a 12-month-old female with a PLAGL2-amplified tumor, had only T1WI sequences without gadolinium contrast available. Another patient, a 25-month-old male also with a PLAGL2-amplified tumor, presented with extensive intratumoral hemorrhage that was partially evacuated. An external ventricular drain (EVD) was placed, followed by a repeat MRI. Analyses were conducted on the second MRI, as the tumor was more discernible in this scan.

A separate case involved a male patient imaged at the age of 17 years for an unspecified cerebellar symptoms. The MRI revealed an ill-defined, non-space occupying lesion in the right dentate nucleus and surrounding cerebellar white matter, characterized by hyperintensity on T2WI and hypointensity on T1WI. Although a stereotactic biopsy was performed, it yielded inconclusive results. Seven months later a clearly visible tumor (PLAGL1) was detected on MRI, which was subsequently used for further analysis in our study.

Tumor localization and imaging features

Results are summarized in Online Supplemental Data, including the distribution according to PLAGL status. Image examples are given in Fig. 1 and in the online figure.

Eight (42%) of the tumors were located infratentorially, with five situated in the brainstem with or without involvement of the cerebellar peduncles, and three in the cerebellar hemispheres with or without affecting the vermis. Ten (53%) were supratentorial, and one was both supra- and infratentorial with three distinct manifestations, located in the right Meckel's cave along the trigeminal nerve and left oculomotor nerve area, as well as the hypothalamus and temporal lobe. Among the supratentorial tumors, two appeared to originate in the lateral and third ventricles. The temporal lobe was implicated in four cases, the insula in three, the basal ganglia in two, the thalamus in two, the parietal lobes in two, and the frontal and occipital lobes each in one case. Most tumors involved more than one region and anatomical compartment, with the exception of pure brainstem or intraventricular tumors. All other tumors affected the cortex and subcortical/periventricular WM. Perifocal edema was mild or intermediate in 14 (74%) cases and pronounced in two (11%). Hydrocephalus was associated with 11 (58%) of the tumors (mild in two, moderate in four, severe in five cases). Five tumors (26%) infiltrated or originated in the ventricular system, while eight (42%) were adjacent to it. The median tumor volume was 50.4 ml (IQR 14.9-107.6 ml).

The larger solid parts of the tumors were mostly of multinodular appearance i.e., consisting of several nodules (e.g., Fig. 1C). The tumors were also characterized by many non-solid components (Fig. 1A-B), or a combination of both solid and non-solid features (Fig. 1D). The signal was heterogeneous in most cases, predominantly slightly hyper-/isointense on T2WI and FLAIR and hypo-/isointense on T1WI in relation to cortical GM. The solid components sometimes contained areas of subtle diffusion restriction with an ADCmean ratio < 1 in 5 of the 14 cases (36%; median ADCmean ratio 0.83, IQR 0.80-0.94), while the remainder (9/14 cases; 64%) had no diffusion restriction with equal or higher ADC values than the contralateral normal-appearing WM (median ADCmean ratio 1.16, IQR 1.11-1.19). ADCmin and ADCmax ratios are given in the Online Supplemental Data. When SWI or T2* series were available (8 cases, whereof one was after hematoma evacuation and EVD placement), they showed susceptibility in parts of the tumor. Whether it was caused by hemorrhage or calcification, could not be reliably determined unless there were unequivocal signs of bleeding with fluid-fluid levels. A 14-year-old girl with a PLAGL1-amplified tumor demonstrated both small calcifications and hemorrhage on CT and SWI (Fig. 1D). In cases where contrast-enhanced series were available, all tumors showed contrast enhancement, typically presenting in a heterogeneous pattern. The enhancement was predominantly mild to intermediate in 10 (53%), and intermediate to strong in 8 (42%) cases, often involving most of the solid tumor component (75-100% in 9 (47%) patients) or all of it (in 6 (32%) patients).

Skull remodeling was observed in 4 (21%) patients, including three cases with a supra- and one with an infratentorial tumors. However, there was no evidence of bony destruction. Notably, not all tumors adjacent to bone showed signs of remodeling. Necrotic regions were present in most tumors (16 cases, 84%), ranging from very small to large, and 47% of the lesions were associated with cysts.

The single dataset with pCASL showed elevated CBF. NAA was considerably decreased, and Choline increased in the three patients who underwent MRS. The Cho/NAA ratio was 10.21, 6.81, and 8.31, respectively. No lactate was detected.

One tumor was metastasized both on MRI and in CSF (female, 8 years and 1 month, PLAGL1-amplified) with one lesion affecting the left uncus, hypothalamus, and oculomotor nerve, the other the right Meckel’s cave. All other tumors were unifocal, although it's important to note that spinal MRI was available only in 63% of the cases.

DISCUSSION

ET, PLAGL is a recently defined embryonal tumor primarily observed in children and adolescents and has not yet been included in the current 2021 WHO Classification of CNS Tumors. In this study, we present the MRI characteristics of this new tumor type for the first time and in the largest cohort so far, to raise awareness within the neuroradiology community.

We found no preferential localization with respect to the supra- or infratentorial space, although PLAGL2-amplified tumors were slightly more common in the supratentorial localization, but the low case number does not allow us to draw reliable conclusions. There were no tumors primarily located in the spinal cord. The supratentorial tumors frequently originated in the temporal and insular regions, extending into the deep grey matter, with two appearing to originate from the ventricular system. However, due to their often substantial size, determining the primary region of origin was challenging. Among the infratentorial tumors, the brainstem was more frequently affected than the cerebellum. At the time of diagnosis, only one tumor was bifocal, indicating dissemination. The remaining tumors were not metastasized, yet only slightly more than half of the cases had undergone spine imaging, preventing a definitive exclusion of spinal dissemination.

In our cohort, a common MRI characteristic of both PLAGL1- and PLAGL2-amplified tumors was their often multinodular structure, accompanied by non-solid components representing cysts and/or necrotic areas. In some cases, the non-solid appearance was more prominent, with only a few, small nodules or non-nodular, solid components present. All tumors exhibited contrast enhancement that was intermediate to strong in the majority of cases. The T2WI and FLAIR signals were heterogeneous, mainly iso- to mildly hyperintense, while the T1WI signal was primarily hypointense, unless there was calcification and/or hemorrhage present, which could alter the signal. Determining the frequency of hemorrhage and/or calcification was challenging, as T2* and SWI series were often not available. When these modalities were accessible, signal loss was consistently present. In most cases, though, we could not ascertain whether they were due to blood products or calcifications. ADC values in the solid parts were equal or higher than in normal-appearing WM in most and lower in the minority of cases. We were not able to identify a discernible pattern that distinguished between PLAGL1- and PLAGL2-amplified tumors. However, this is not surprising given the relatively low number of cases.

In our analysis, some ET, PLAGL exhibited MRI characteristics seen in low-grade tumors, such as T2WI hyperintensity and little or no diffusion restriction. Like other embryonal tumors, including medulloblastoma, ET, PLAGL are histopathologically defined by primitive, embryonal-like cells with numerous mitoses (4). Generally, such tumors exhibit T2WI hypointensity in at least parts of the lesion and demonstrate diffusion restriction, suggesting high cell density. However, these expected characteristics were rarely observed in our cases. Other embryonal CNS tumors, such as ATRT, ETMR, and CNS Neuroblastoma-FOXR2 (6–9) also show high proliferation rates and can exhibit T2WI hyperintensity. However, they typically display strong diffusion restriction, which is in contrast to most ET, PLAGL in our cohort.

The reasons behind the relatively high T2WI signal and ADC values in these tumors remain unknown. It is well-known that DWI signals are not only influenced by cellularity and the nucleus-cytoplasm ratio, but also by myelin content (10), cell morphology, water compartments, and architectural variances in the respective anatomical region (11), which is not fully captured by standard DWI. Advanced imaging techniques, such as neurite orientation dispersion and density imaging or diffusion kurtosis imaging, might be required to understand these aspects more comprehensively (12,13). In our study, the presence of numerous necrotic regions, detectable both histologically and in MRI, could contribute to the T2WI hyperintensity and relatively high ADC values. This observation underscores the complexity and variability in imaging characteristics of ET, PLAGL and other embryonal tumors. ADC values are traditionally regarded as a key parameter for differentiating high-grade from low-grade tumors and are particularly useful in distinguishing posterior fossa tumors in children (14), but the increasingly detailed 2021 WHO Classification of CNS Tumors may challenge some of the conventional imaging principles.

To date, the MRI phenotype of ET, PLAGL has not been systematically described. A recent case report of a 4-year-old girl with a PLAGL1-amplified tumor describes an exophytic pontine tumor with T2WI hypointensity, diffusion restriction, and moderate homogeneous enhancement (15). While these findings seem at odds with our results, the images provided closely match those from cases presented here; we would have characterized the tumor as T2WI isointense to cortical GM with intermediate, slightly heterogeneous enhancement, and no diffusion restriction according to our definition. However, a definitive assessment can obviously only be made with access to the full dataset and highlights the need for standardized imaging criteria within the community. Additionally, a recent study by Tauziède-Espariat et al. discussed two patients with PLAG1 fusions that show epigenetic, radiological, and histopathological similarities to ET, PLAGL (16). In their study, while a detailed description is not provided, the images displayed similar characteristics such as T2WI iso- to hyperintensity, partially heterogeneous enhancement, signal loss on SWI, and no perifocal edema. However, based on just two cases, it is challenging to conclusively group tumors with PLAG1 fusion and PLAGL1/2 amplification together. Furthermore, as observed in our study, reliably distinguishing these tumors from other, particularly embryonal, tumors remain difficult.

While patient age at diagnosis can be a helpful factor in narrowing down the differential diagnosis in other embryonal tumors, it is less clear ET, PLAGL. For example, ATRT typically presents in children under the age of 2 years (17), which is similar to PLAGL2-amplified tumors (median age 1.9 years). Patients with PLAGL1-amplified tumors, with a median age of 7.3 years in our cohort, fall into the same age group as those with CNS Neuroblastoma-FOXR2 (median age 5-8 years) and are older than patients with CNS tumors with BCOR-ITD (median age 4 years) or ETMR (median age 2.5 years) (18). The age of patients with PLAGL2-amplified tumors can also overlap with that of patients with BRAF V600E-mutated astrocytomas, a low-grade glioma that can have similar imaging characteristics with T2WI hyperintensity and occasional diffusion restriction (19). However, in our cohort, PLAGL1-amplified tumors could not be differentiated from PLAGL2-amplified tumors based on imaging. Therefore, they must be summarized as a group with a median age of 3 years, which is similar to that of patients with ETMR. The imaging characteristics of ETMR, however, are distinct, typically characterized by T2WI hyperintensity, weak enhancement, and consistent diffusion restriction (8). Comparative studies on ADC values have been conducted on common pediatric posterior fossa tumors, including medulloblastoma, ependymoma, ATRT, pilocytic astrocytoma, and diffuse midline glioma (20–22) but, to our knowledge, are still lacking for rare embryonal tumors. Based on known comparative studies with common pediatric brain tumors, ET, PLAGL appears to have less diffusion restriction than medulloblastomas and ATRT, but more than pilocytic astrocytomas, and may be comparable to that of ependymomas (20,22).

This study has several limitations. Firstly, the analysis was conducted retrospectively and on a relatively small number of cases, a common challenge when dealing with rare, newly described tumor entities. This underscores the importance of close collaboration between centers to collect sufficient cases, especially as tumor classification becomes increasingly detailed and results in inherently low case numbers. Another limitation is the variability and sometimes incompleteness of the MRI data, e.g., missing SWI, T2*, or DWI, which hinders the systematic analysis. The adoption of standardized imaging protocols across centers treating pediatric tumor patients would significantly mitigate this issue (23). Additionally, the limited availability of advanced imaging techniques in our dataset represents a considerable constraint.

Table 1: Patients demographics and *PLAGL1/2* status.

	Sex (female/male)	age (in years; median, IQR)
all	10/9 (53%/47%)	3 (1.8-5.9)
PLAGL1-amplified: 10 cases (53%)	7/3 (70%/30%)	7.3 (3.9-14)
PLAGL2- amplified: 9 cases (47%)	3/6 (33%/66%)	1.9 (1.3-2.1)

CONCLUSIONS

In conclusion, we present the most comprehensive MRI data series to date on ET, PLAGL, a rare and recently identified embryonal tumor in children and adolescents. It is not possible to distinguish between PLAGL1- and PLAGL2-amplified tumors based on imaging, nor can ET, PLAGL be differentiated from other embryonal CNS tumors using MRI. Our study contributes to the evolving characterization of new tumor entities, a process increasingly refined by advances in DNA methylation profiling, copy number analysis, and DNA/RNA sequencing. We advocate for enhanced collaboration between centers treating these patients, which is crucial for deepening our understanding of emerging tumor entities.

ACKNOWLEDGMENTS

Language editing assistance was provided by the large language model ChatGPT.

REFERENCES

1. 1. Louis DN, Perry A, Wesseling P, Brat DJ, Cree IA, Figarella-Branger D, et al. The 2021 WHO Classification of Tumors of the Central Nervous System: a summary. Neuro-Oncol. 2021 Aug 2;23(8):1231–51.
2. 2. Alhalabi KT, Stichel D, Sievers P, Peterziel H, Sommerkamp AC, Sturm D, et al. PATZ1 fusions define a novel molecularly distinct neuroepithelial tumor entity with a broad histological spectrum. Acta Neuropathol (Berl). 2021;142(5):841–57.
3. 3. Sievers P, Henneken SC, Blume C, Sill M, Schrimpf D, Stichel D, et al. Recurrent fusions in PLAGL1 define a distinct subset of pediatric-type supratentorial neuroepithelial tumors. Acta Neuropathol (Berl). 2021 Nov 1;142(5):827–39.
4. 4. Keck MK, Sill M, Wittmann A, Joshi P, Stichel D, Beck P, et al. Amplification of the PLAG-family genes—PLAGL1 and PLAGL2—is a key feature of the novel tumor type CNS embryonal tumor with PLAGL amplification. Acta Neuropathol (Berl). 2023 Jan 1;145(1):49–69.
5. 5. Adnani L, Dixit R, Chen X, Balakrishnan A, Modi H, Touahri Y, et al. Plag1 and Plagl2 have overlapping and distinct functions in telencephalic development. Biol Open. 2018 Nov 26;7(11):bio038661.
6. 6. Tietze A, Mankad K, Lequin MH, Ivarsson L, Mirsky D, Jaju A, et al. Imaging Characteristics of CNS Neuroblastoma-FOXR2: A Retrospective and Multi-Institutional Description of 25 Cases. AJNR Am J Neuroradiol. 2022 Oct;43(10):1476–80.
7. 7. Jin B, Feng XY. MRI features of atypical teratoid/rhabdoid tumors in children. Pediatr Radiol. 2013 Aug 1;43(8):1001–8.
8. 8. Dangouloff-Ros V, Tauziède-Espariat A, Roux CJ, Levy R, Grévent D, Brunelle F, et al. CT and Multimodal MR Imaging Features of Embryonal Tumors with Multilayered Rosettes in Children. AJNR Am J Neuroradiol. 2019 Apr;40(4):732–6.
9. 9. D'Arco F, Khan F, Mankad K, Ganau M, Caro-Dominguez P, Bisdas S. Differential diagnosis of posterior fossa tumours in children: new insights. Pediatr Radiol. 2018 Dec;48(13):1955–63.
10. 10. Harkins KD, Does MD. Simulations on the Influence of Myelin Water in Diffusion-Weighted Imaging. Phys Med Biol. 2016 Jul 7;61(13):4729–45.
11. 11. Radhakrishnan H, Shabestari SK, Blurton-Jones M, Obenaus A, Stark CEL. Using Advanced Diffusion-Weighted Imaging to Predict Cell Counts in Gray Matter: Potential and Pitfalls. Front Neurosci. 2022 Jun 3;16:881713.
12. 12. Tang L, Zhou XJ. Diffusion MRI of Cancer: from Low to High b-Values. J Magn Reson Imaging JMRI. 2019 Jan;49(1):23–40.
13. 13. Tietze A, Hansen MB, Ostergaard L, Jespersen SN, Sangill R, Lund TE, et al. Mean Diffusional Kurtosis in Patients with Glioma: Initial Results with a Fast Imaging Method in a Clinical Setting. AJNR Am J Neuroradiol. 2015 Aug;36(8):1472–8.
14. 14. Alves C a. PF, Löbel U, Martin-Saavedra JS, Toescu S, Tsunemi MH, Teixeira SR, et al. A Diagnostic Algorithm for Posterior Fossa Tumors in Children: A Validation Study. Am J Neuroradiol [Internet]. 2021 Mar 4 [cited 2021 Mar 27]; Available from: http://www.ajnr.org/content/early/2021/03/04/ajnr.A7057
15. 15. Maldonado F, Geraldo AF, Guarnizo A, Fernández-Ponce N, Baroni L, Rugilo C. Central nervous system embryonal tumor with PLAGL1 amplification: a case report of a novel entity focusing on imaging findings. Childs Nerv Syst [Internet]. 2024 Apr 20 [cited 2024 Apr 28]; Available from: https://doi.org/10.1007/s00381-024-06422-8
16. 16. Tauziède-Espariat A, Siegfried A, Nicaise Y, Dghayem D, Laprie A, Lubrano V, et al. PLAG1 fusions extend the spectrum of PLAG(L)-altered CNS tumors. Acta Neuropathol (Berl). 2023 Dec;146(6):841–4.
17. 17. Ostrom QT, Chen Y, M. de Blank P, Ondracek A, Farah P, Gittleman H, et al. The descriptive epidemiology of atypical teratoid/rhabdoid tumors in the United States, 2001–2010. Neuro-Oncol. 2014 Oct;16(10):1392–9.
18. 18. Gojo J, Kjaersgaard M, Zezschwitz BV, Capper D, Tietze A, Kool M, et al. Rare embryonal and sarcomatous central nervous system tumours: State-of-the art and future directions. Eur J Med Genet. 2023 Jan;66(1):104660.
19. 19. Trasolini A, Erker C, Cheng S, Crowell C, McFadden K, Moineddin R, et al. MR Imaging of Pediatric Low-Grade Gliomas: Pretherapeutic Differentiation of BRAF V600E Mutation, BRAF Fusion, and Wild-Type Tumors in Patients without Neurofibromatosis-1. AJNR Am J Neuroradiol. 2022 Aug;43(8):1196–201.
20. 20. Phuttharak W, Wannasarnmetha M, Waraaswapati S, Yuthawong S. Diffusion MRI in Evaluation of Pediatric Posterior Fossa Tumors. Asian Pac J Cancer Prev APJCP. 2021 Apr;22(4):1129–36.
21. 21. Novak J, Zarinabad N, Rose H, Arvanitis T, MacPherson L, Pinkey B, et al. Classification of paediatric brain tumours by diffusion weighted imaging and machine learning. Sci Rep. 2021 Feb 4;11(1):2987.
22. 22. Chen D, Lin S, She D, Chen Q, Xing Z, Zhang Y, et al. Apparent Diffusion Coefficient in the Differentiation of Common Pediatric Brain Tumors in the Posterior Fossa: Different Region-of-Interest Selection Methods for Time Efficiency, Measurement Reproducibility, and Diagnostic Utility. J Comput Assist Tomogr. 2023 Apr;47(2):291.
23. 23. Avula S, Peet A, Morana G, Morgan P, Warmuth-Metz M, Jaspan T, et al. European Society for Paediatric Oncology (SIOPE) MRI guidelines for imaging patients with central nervous system tumours. Childs Nerv Syst ChNS Off J Int Soc Pediatr Neurosurg. 2021 Aug;37(8):2497–508.

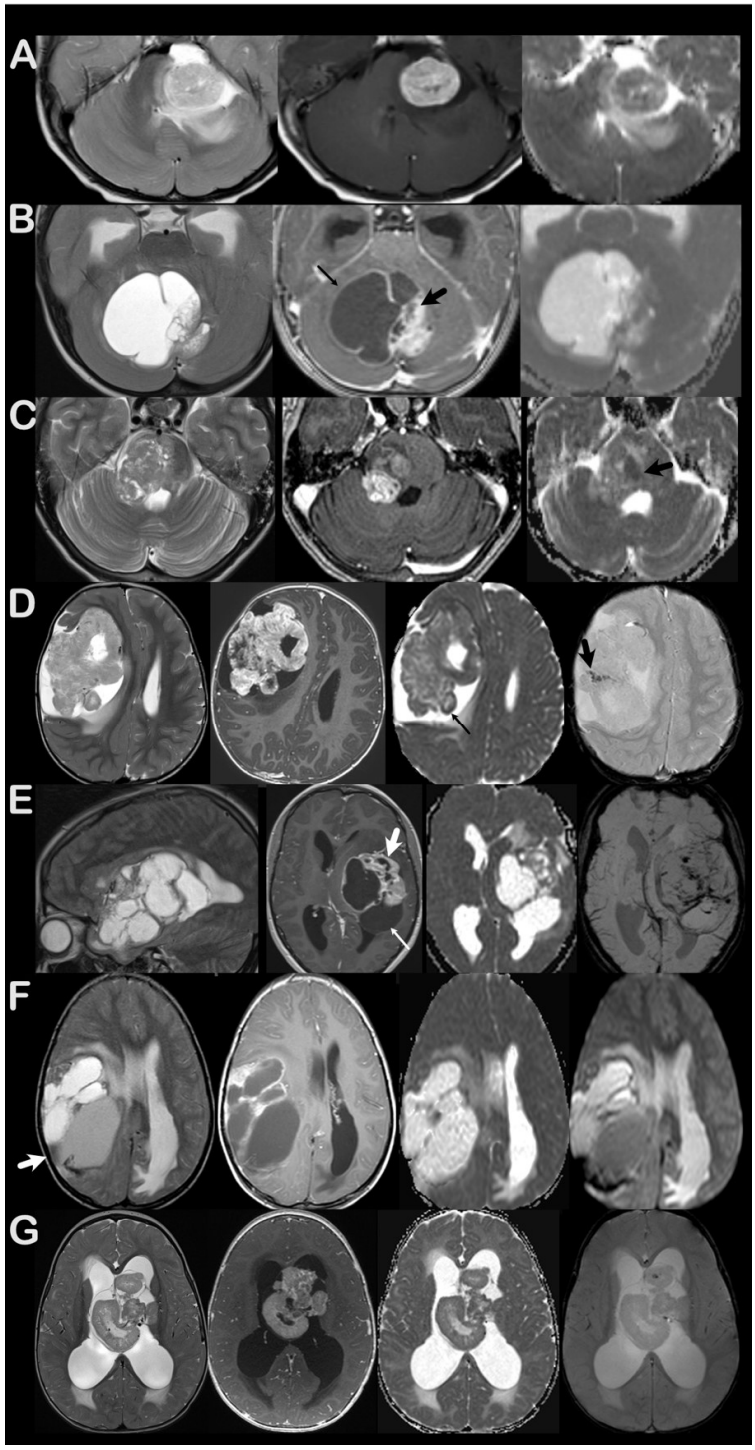

Online figure: Image examples of *PLAGL1*- and *PLAGL2*-amplified tumors.

A: 25-month-old male with a *PLAGL2*-amplified tumor in the left side of the pons, extending into the cerebello-pontine angle with T2WI hyperintensity, intermediate to strong, inhomogeneous enhancement, and almost no convincing diffusion restriction(ADC_{mean} ratio 1.16). There is intermediate to strong, perifocal edema. (From left to right: T2WI, contrast enhanced T1WI, ADC).

B: 21-month-old girl with a *PLAGL1*-amplified tumor involving the right cerebellar hemisphere and the vermis with large, thin-walled cysts and small, thick-walled necrotic areas (thin and thick, black arrows, second image). The solid components are T2WI hyper- to isointense, show intermediate to strong enhancement, and have no diffusion restriction (ADC_{mean} ratio 1.04). (From left to right: T2WI, contrast enhanced T1WI, ADC).

C: 14-year-old male with a *PLAGL1*-amplified tumor in the right side of the pons and the right, middle cerebellar peduncle. It has a multinodular appearance, is T2WI isointense, and shows weak to intermediate enhancement after contrast administration. ADC values are predominantly relatively high, but are decreased in some areas (black arrow, last image; ADC_{mean} ratio 0.80). (From left to right: T2WI, contrast enhanced T1WI, ADC).

D: 22-month-old male with a large, multinodular, T2WI hyper- and isointense *PLAGL2*-amplified tumor with very inhomogeneous enhancement, slightly decreased ADC values in some regions (thin black arrow, third image; ADC_{mean} ratio 0.94), and subtle susceptibilities because of calcifications or hemorrhage (black arrow, fourth image). (From left to right: T2WI, contrast enhanced T1WI, ADC, T2*).

E: 17-year-old female with a *PLAGL1*-amplified tumor in the left temporal lobe, partly infiltrating the basal ganglia and causing midline shift, compression of the left and dilation of the right lateral ventricle. There are both thin-walled cysts and thick-walled necroses (thin and thick arrows, second image). The solid part is of multinodular appearance and shows no obvious diffusion restriction (ADC_{mean} ratio 1.19) as well as multiple susceptibilities. (From left to right: T2WI, contrast enhanced T1WI, ADC, SWI).

F: 3-year-old female with a *PLAGL1*-amplified tumor in the right temporo-parietal lobes, abutting, but not infiltrating the right lateral ventricle. The solid components are T2WI iso- to hypointense and enhance strongly after contrast administration. The large, posteromedial cyst is relatively hypointense on T2WI (first image) and on DWI-B0 (last image), and the subtle fluid-fluid level is highly suggestive of a recent hemorrhage (white arrow, first image). There is diffusion restriction (ADC_{mean} ratio 0.83). (From left to right: T2WI, contrast enhanced T1WI, ADC, DWI-B0).

G: 15-month-old male with a multinodular, mostly T2WI isointense, partly necrotic *PLAGL2*-amplified tumor that arises in the fornix and the lateral ventricles, causing hydrocephalus of medium degree. There is heterogeneous, predominantly intermediate enhancement, diffusion restriction (ADC_{mean} ratio 0.75), and very subtle susceptibilities. (From left to right: T2WI, contrast enhanced T1WI, ADC, T2*).

Online Table: Imaging features, listed separately for *PLAGL1*- and *PLAGL2*-amplified tumors.

	PLAGL1-amplified	*PLAGL2*-amplified
supratentorial	4 (40%)	6 (67%)
infratentorial	5 (50%)	3 (33%)
supra-/infratentorial	1 (10%)	0
right; left; bilateral	5; 3; 2 (50%; 30%; 20%)	2; 5; 2 (22%; 56%; 22%)
intraventricular or infiltrating the ventricular system	1 (10%)	4 (44%)
abutting the ventricular system	4 (40%)	4 (44%)
edema: no; little; intermediate; much	2; 3; 3; 2 (20%; 30%; 30%; 20%)	1; 4; 4; 0 (11%; 44%; 44%; 0%)
hydrocephalus: no; mild; moderate; severe	5; 0; 3; 2 (50%; 0%; 30%; 20%)	3; 2; 1; 3 (33%; 22%; 11%; 33%)
median tumor volume [ml] (IQR)	48.0 (21.9-94.3)	64.8 (10.9-111.0)
T2w: only hyper- and/or isointense; hyper-/isointense with hypointense components	9; 1 (90%; 10%)	5; 3 (62.5%; 37.5%)
T1w: hypointense; isointense; hypo- and isointense	6; 1; 3 (60%; 10%; 30%)	7; 0; 1 (87.5%; 0%; 12.5%)
FLAIR: hyper- and/or isointense; hyper-/iso-/hypointense	9; 1 (90%; 10%)	5; 2 (71.4%; 28.6%)
SWI/T2* hypointensity	5 (100%)	3 (100%)
strength of contrast enhancement: none; mild/intermediate; intermediate/strong	0; 7; 3 (0%; 70%; 30%)	0; 2; 6 (0%; 25%; 75%)
extent of contrast enhancement: 0%; 0-25%; 25-50%; 50-75%; 75-100%; 100%	0; 1; 0; 0; 7; 2 (0%; 10%; 0%; 0%; 70%; 20%)	0; 0; 1; 1; 2; 4 (0%; 0%; 12.5%; 12.5%; 25%; 75%)
median ADC_{mean} ratio	1.11 (1.04-1.19)	1.0 (0.94-1.0)
median ADC_{min} ratio	1.12 (1.08-1.19)	0.96 (0.79-1.08)
median ADC_{max} ratio	1.10 (1.03-1.30)	1.05 (0.98-1.16)
skull remodeling	3 (30%)	1 (11.1%)
necrosis	9 (90%)	7 (77.8%)
cysts	6 (60%)	3 (33.3%)